

Supplemental information

Amelioration of SARS-CoV-2 infection by

ANO6 phospholipid scramblase inhibition

Ju-Ri Sim, Dong Hoon Shin, Pil-Gu Park, So-Hyeon Park, Joon-Yong Bae, Youngchae Lee, Dha-Yei Kang, Ye Jin Kim, Sowon Aum, Shin Hye Noh, Su Jin Hwang, Hye-Ran Cha, Cheong Bi Kim, Si Hwan Ko, Sunghoon Park, Dongkyu Jeon, Sungwoo Cho, Gee Eun Lee, Jeonghun Kim, Young-hye Moon, Jae-Ouk Kim, Jae-Sung Nam, Chang-Hoon Kim, Sungmin Moon, Youn Wook Chung, Man-Seong Park, Ji-Hwan Ryu, Wan Namkung, Jae Myun Lee, and Min Goo Lee

Supplemental Information for

Amelioration of SARS-CoV-2 infection by ANO6 phospholipid scramblase inhibition

Ju-Ri Sim^{1,8}, Dong Hoon Shin^{1,8}, Pil-Gu Park^{2,8}, So-Hyeon Park^{3,8}, Joon-Yong Bae^{4,8},
Youngchae Lee¹, Dha-Yei Kang¹, Ye Jin Kim¹, Sowon Aum¹, Shin Hye Noh^{1,7}, Su Jin
Hwang², Hye-Ran Cha², Cheong Bi Kim², Si Hwan Ko², Sunghoon Park², Dongkyu
Jeon³, Sungwoo Cho³, Gee Eun Lee⁴, Jeonghun Kim⁴, Young-hye Moon⁵, Jae-Ouk
Kim⁵, Jae-Sung Nam⁶, Chang-Hoon Kim⁶, Sungmin Moon⁷, Youn Wook Chung⁷, Man-
Seong Park⁴, Ji-Hwan Ryu^{7,*}, Wan Namkung^{3,*}, Jae Myun Lee^{2,*}, Min Goo Lee^{1,7,9,*}

This PDF file includes:

Figure S1 to S7

Table S1

Videos S1 to S8

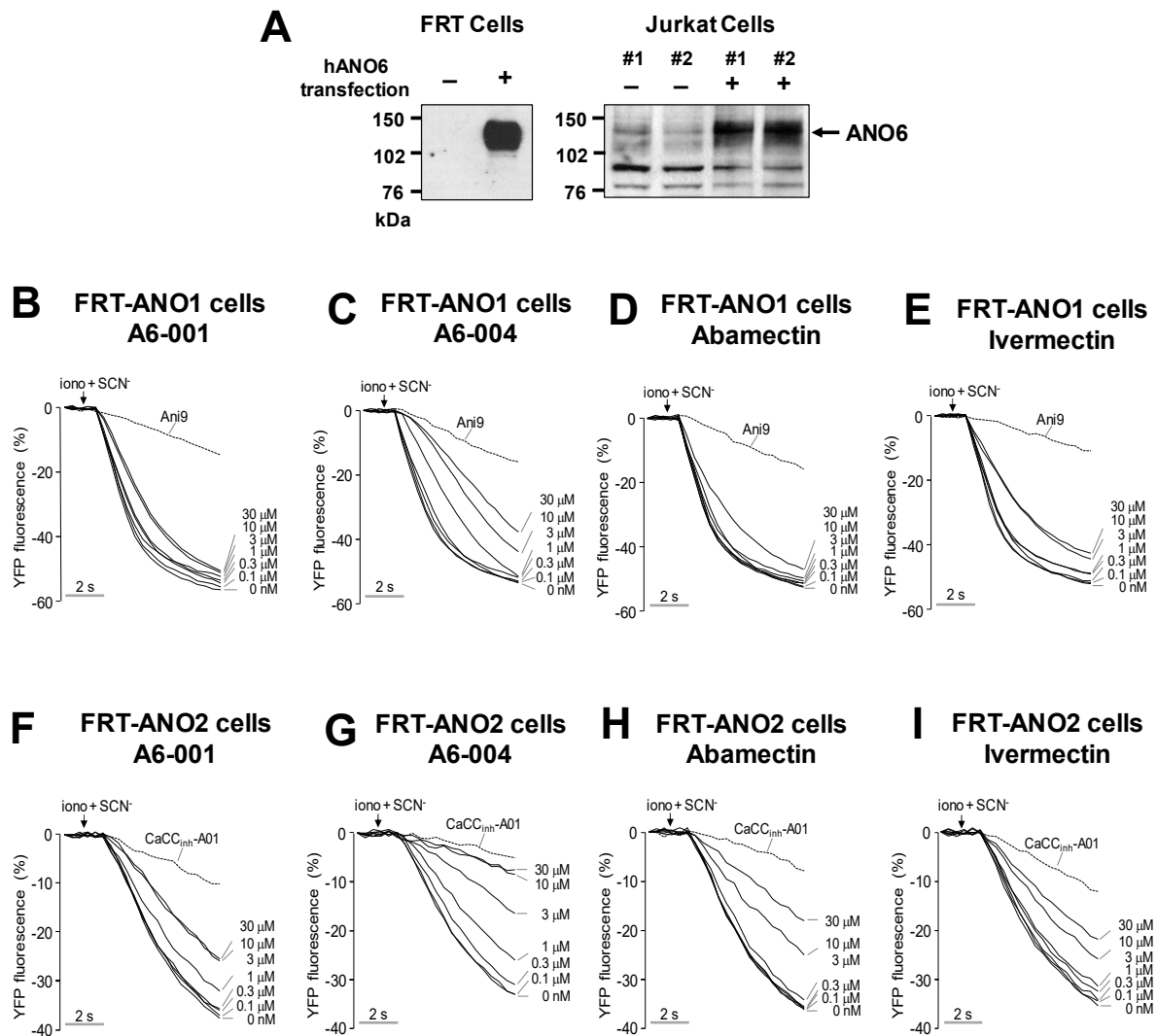


Figure S1. Expression of ANO6 in FRT cells and effects of ANO6 inhibitors on ANO1 and ANO2, Related to Figure 1.

(A) Immunoblotting of ANO6 in FRT and Jurkat cells with exogenous ANO6 expression. The FRT cells were stably transfected with pcDNA3.1-ANO6 (variant 5) and the Jurkat suspension cells were transiently transfected with the same plasmid using a NEPA21 Super Electroporator as described in Method Details. Jurkat cells also expressed a basal level of endogenous ANO6.

(B-E) ANO1 anion channel activity was measured in FRT cells expressing human ANO1 and the halide sensor YFP. Compounds were applied 10 min prior to ANO1 activation by 10 μ M ionomycin (iono). Permeation of SCN^- through ANO1 anion channels quenches the YFP fluorescence. ANO1 anion channels were fully inhibited by An9 (10 μ M). A summary of the dose response of ANO6 inhibitors on the ANO1 anion channel activity is shown in Figure 1G.

(F-I) ANO2 anion channel activities were measured in FRT cells expressing human ANO2 and the halide sensor YFP. ANO2 anion channels were fully inhibited by CaCCinh-A01 (30 μ M). A summary of the dose response of ANO6 inhibitors on the ANO2 anion channel activity is shown in Figure 1H.

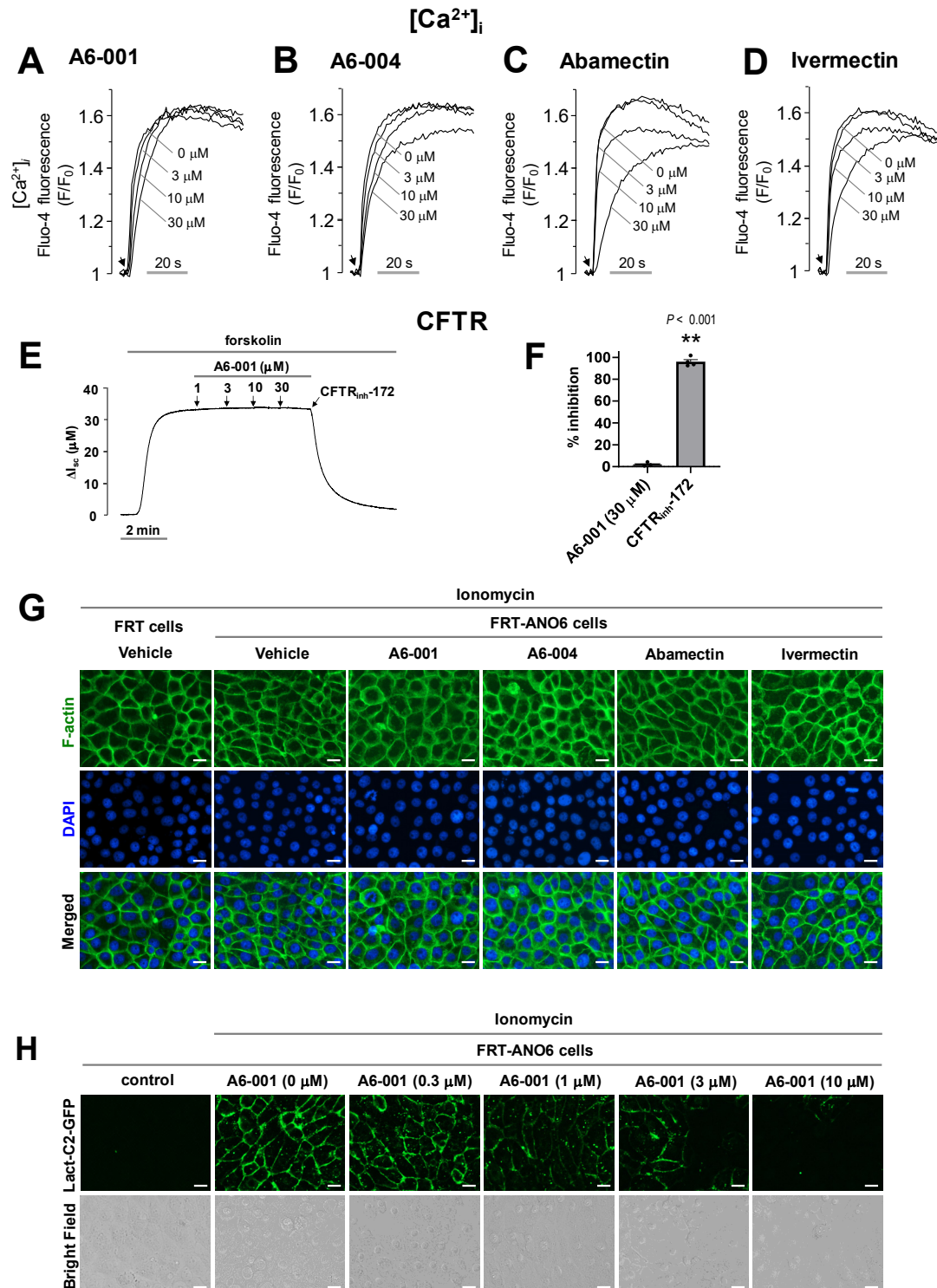


Figure S2. Effects of ANO6 inhibitors on cytosolic Ca^{2+} levels, CFTR Cl^- currents, and cell morphology, Related to Figure 2.

(A-D) Intracellular calcium ($[Ca^{2+}]_i$) was monitored using the Fluo-4 NW calcium indicator. The FRT cells were treated with the indicated concentrations of compounds for 10 min and then ionomycin (10 μ M) was applied to evoke $[Ca^{2+}]_i$ elevation. Representative traces of intracellular calcium responses pretreated with A6-001 (A), A6-004 (B), abamectin (C), and ivermectin (D) are shown. Three independent experiments yielded similar results.

(E and F) Effects of A6-001 on CFTR Cl^- channel activity. The apical membrane short-circuit currents (I_{sc}) were measured in FRT-CFTR cells cultured on a permeable support. The basolateral membrane was permeabilized with amphotericin B (250 μ g/ml). CFTR was stimulated using forskolin (20 μ M) and blocked by CFTR_{inh}-172 (20 μ M). Representative I_{sc} measurements are shown in (E) and a summary of the current inhibition rates by A6-001 (30 μ M) and CFTR_{inh}-172 (20 μ M) is provided in (F, mean \pm SEM, n = 4, $**P < 0.01$ using a two-tailed Student's *t*-test).

(G) Effects of ANO6 inhibitors on cytoskeletal structure and on the nuclei were analyzed using F-actin and DAPI staining. The newly identified ANO6 inhibitors do not noticeably affect the cell and nuclear morphologies. Three independent experiments showed similar results.

(H) The dose responses of A6-001 on ANO6 PS scramblase inhibition were analyzed. PS externalization was assessed via the fluorescence intensity of Lact-C2-GFP. A summary of the multiple experiments is shown in Figure 2F. Scale bar: 10 μ m.

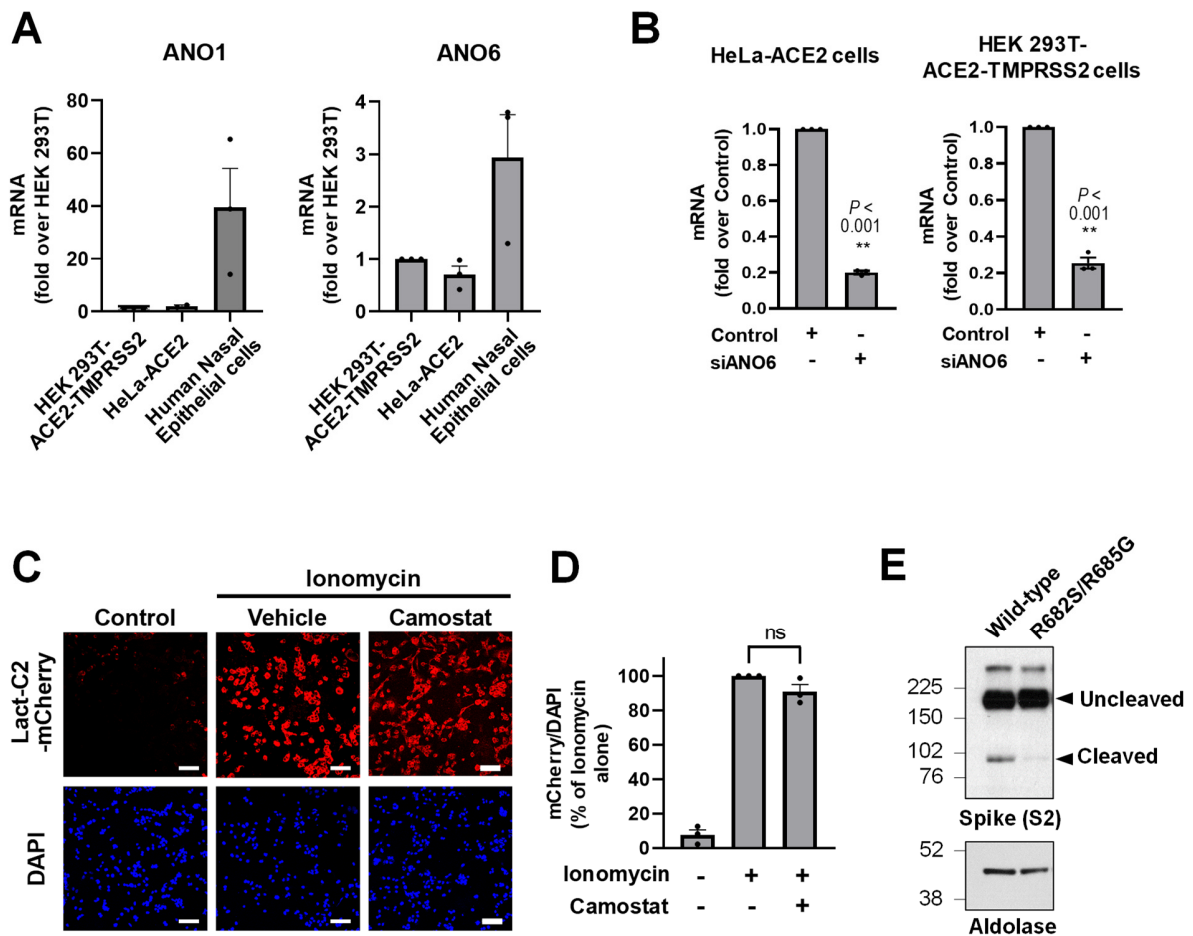


Figure S3. Supporting results for Figures 3 and 4, Related to Figures 3 and 4.

(A) mRNA quantification of ANO1/TMEM16A and ANO6/TMEM16F using qPCR. ANO1 is highly expressed in the primarily cultured human nasal epithelial (HNE) cells (left panel). The ANO6 expression levels in HEK-293T, HeLa, and HNE cells are shown in the right panel.

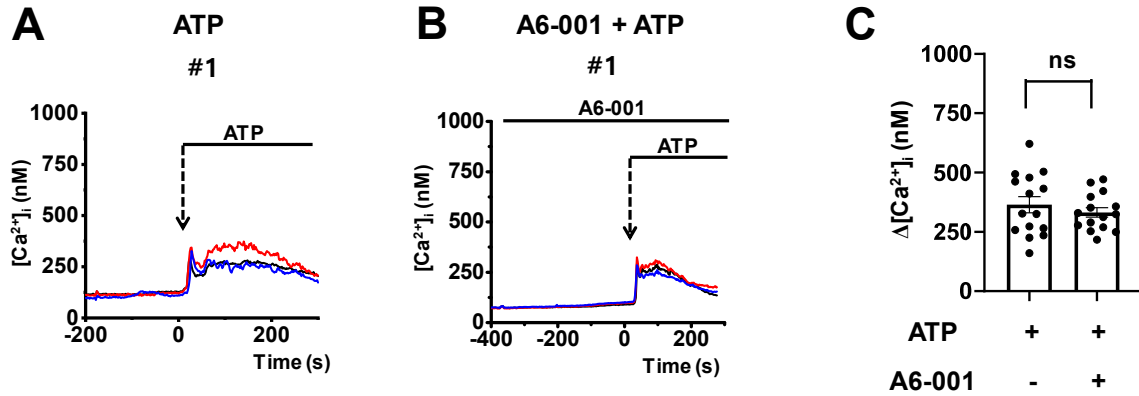
(B) The silencing of ANO6 mRNA via treatment with siRNAs against ANO6 was analyzed in HeLa-ACE2 cells and HEK 293T-ACE2-TMPRSS2 cells using qPCR. Cells were treated with scrambled or ANO6 siRNAs (100 nM in each case) for 24 h (n = 3).

(C and D) Effects of camostat on ionomycin (10 μ M, 10 min)-induced PS scrambling. The trypsin inhibitor camostat (100 μ M) was applied 1-h prior to ionomycin application. Representative images are shown in (C) and the summarized results of multiple experiments are depicted in (D, n = 3). Scale bar: 50 μ m.

(E) Immunoblot analysis of the SARS-CoV-2 Spike glycoprotein. The cell lysates of wild-type and R682S/R685G SARS2-PsV infected HEK 293T cells were blotted with primary antibodies against the S2 domain of Spike and aldolase A. The R682S/R685G mutant Spike proteins do not exhibit a protease cleaved form.

Bar graph data are shown as the mean \pm SEM. Data were analyzed using a two-tailed Student's *t*-test (B) or one-way analysis of variance followed by Tukey's multiple comparison test (D). ***P* < 0.01, ns: not significant.

HEK 293T-ACE2-TMPRSS2 cells



Calu-3 cells

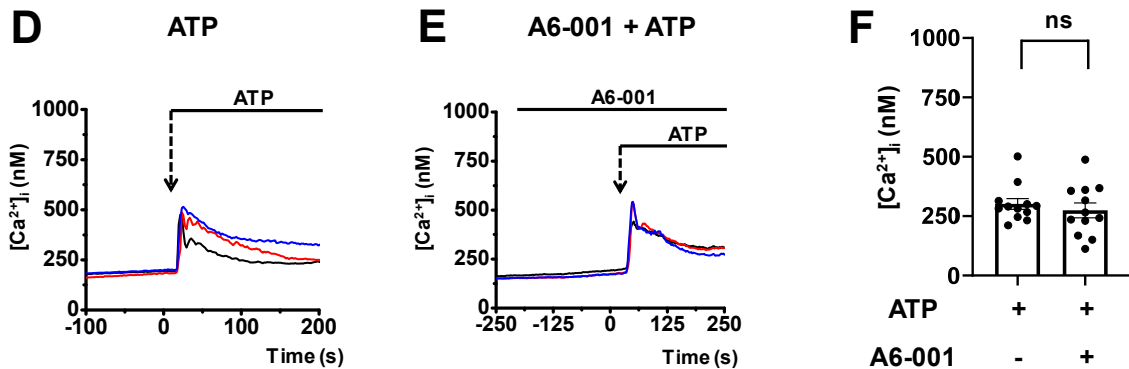


Figure S4. A6-001 does not affect the ATP-induced Ca^{2+} response, Related to Figure 5.

(A-C) Purinergic agonist (ATP, 100 μM)-induced Ca^{2+} response in HEK 293T-ACE2-TMPRSS2 cells was monitored in the absence and presence of A6-001 (10 μM). Representative traces (two each) are shown in (A) and (B), respectively. A summary of $\Delta[\text{Ca}^{2+}]_i$ increase is presented in (C, $n = 15$).

(D-E) ATP-induced Ca^{2+} response (100 μM) in Calu-3 cells was monitored in the absence and presence of A6-001 (10 μM). Representative traces are shown in (D) and (E), respectively. A summary of $\Delta[\text{Ca}^{2+}]_i$ increase is presented in (F, $n = 12$).

Data were analyzed using a two-tailed Student's t -test. ns: not significant.

SARS-CoV-2 (0.01 MOI), 48 h, supernatant

Vero cells

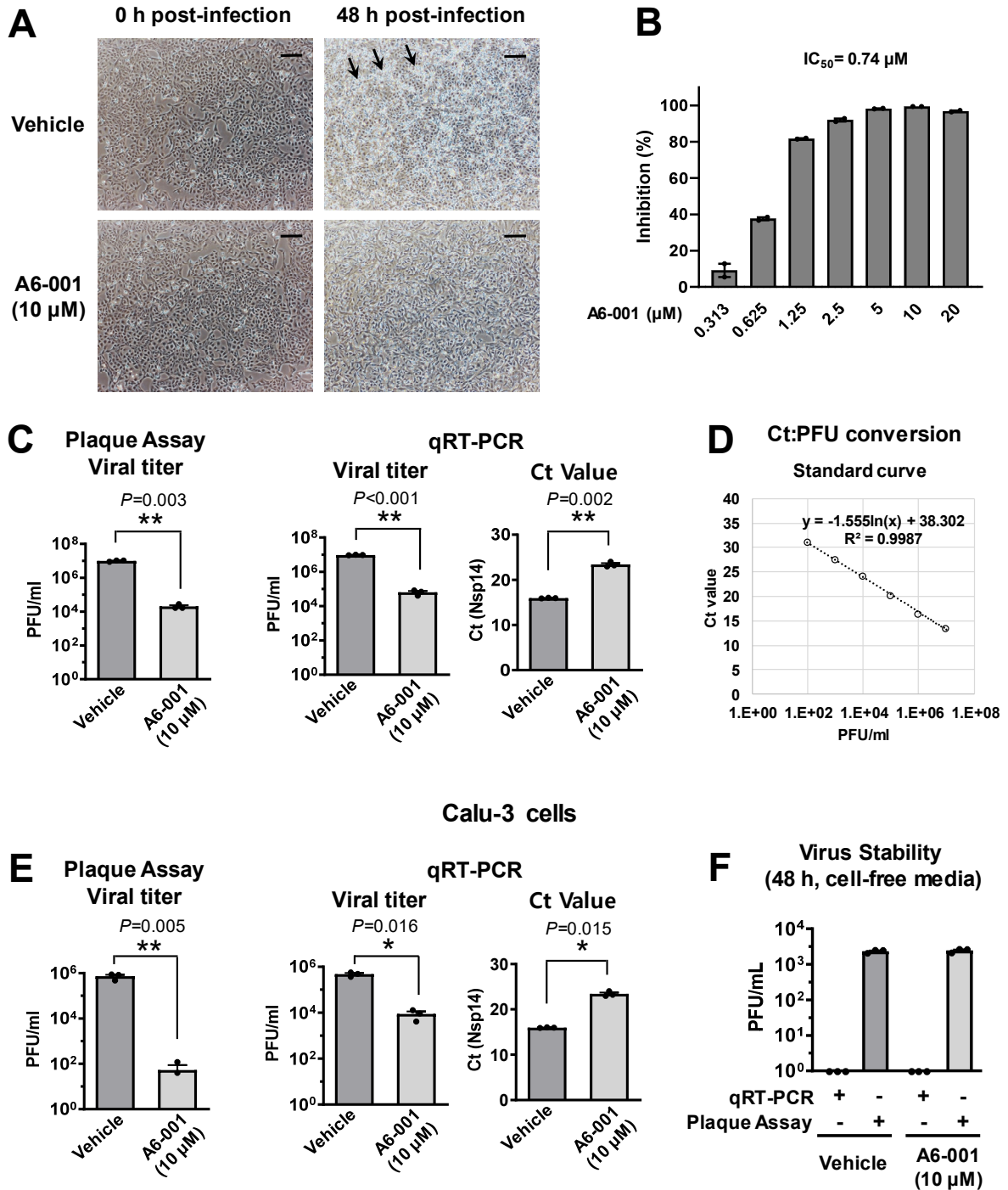


Figure S5. Effects of A6-001 on the viral replications of SARS-CoV-2 in Vero and Calu-3 cells, Related to Figure 7.

(A and B) Viral replication of SARS-CoV-2 in Vero cells with an infection dose of 0.01 MOI (ten times higher than that in Figure 7C-7E). In the light microscopic analysis, A6-001 reduced the virus-induced cytolysis (A, 48 h post-infection; arrows indicate cytolytic areas. Scale bar: 100 μ m). The IC_{50} value of A6-001 at 48 h post-infection is presented in (B, n = 2 at each concentration).

(C and D) The side-by side parallel data for RNA accumulations and output virus titers by plaque assay in Vero cells infected with SARS-CoV-2 (0.01 MOI). The plaque assay results indicate that A6-001 (10 μ M, 48 h) induced a 1/500 virus reduction (9.8×10^6 vs. 2.0×10^4 PFU/ml, n = 3), while the qPCR results represent a 1/150 reduction (9.6×10^6 vs. 6.4×10^4 PFU/ml, n = 3). The qPCR threshold cycle (Ct) values were converted into viral titer (PFU/ml). An example of standard curve for the conversion of Ct into viral titer is shown in (D).

(E and F) The side-by side parallel data for RNA accumulations and output virus titers by plaque assay in Calu-3 cells infected with SARS-CoV-2 (0.01 MOI). The plaque assay results indicate that A6-001 (10 μ M, 48 h) induced a 1/14,000 virus reduction (7.3×10^5 vs. 5.3×10^1 PFU/ml, n = 3), while the qPCR results represent a 1/50 reduction (4.7×10^5 vs. 8.8×10^3 PFU/ml, n = 3). Virus stability was analyzed after a 48-h incubation in cell-free media using the samples collected from culture supernatant at 0 h post-infection (F, n = 3). The SARS-CoV-2 loses viability after a 48-h incubation in cell-free media. Note that qPCR detects non-viable viruses.

Bar graph data are shown as the mean \pm SEM. * $P < 0.05$, ** $P < 0.01$: Data were analyzed using a two-tailed Student's *t*-test.

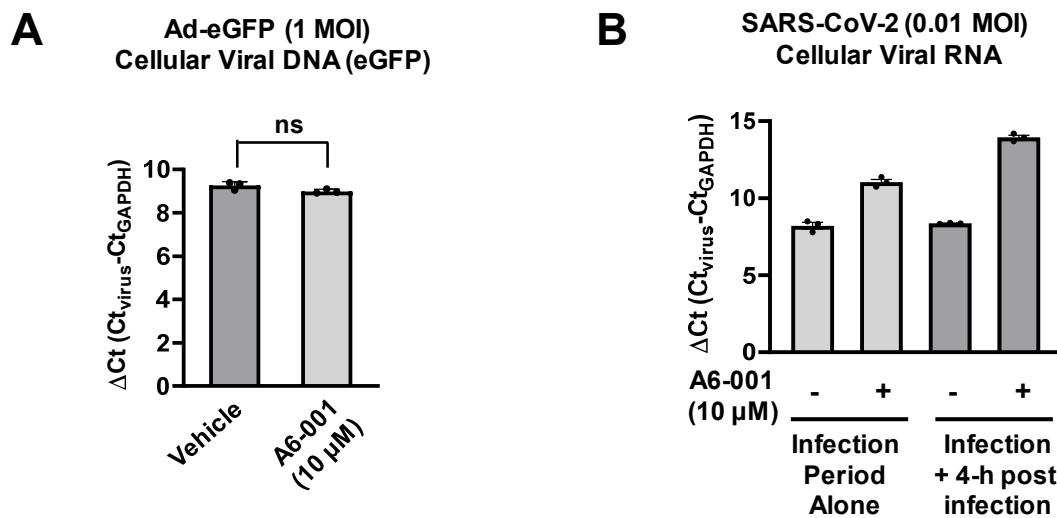


Figure S6. Effects of A6-001 on the viral replications of SARS-CoV-2 and adenoviruses, Related to Figure 7.

(A) Effects of A6-001 on the viral replications of non-enveloped adenoviruses were analyzed. HEK 293T cells were infected with the recombinant eGFP adenovirus (Ad-eGFP, 1 MOI) and incubated for 48 h. The quantity of viral transgene was quantified using qPCR assays with cellular DNA samples. A6-001 (10 μM) did not affect replications of the recombinant adenovirus ($n = 3$).

(B) Vero cells were infected with SARS-CoV-2 (0.01 MOI) and cellular viral RNAs were quantified using qPCR at 4 h post-infection. A6-001 (10 μM) was treated during the infection period alone (for 2-h pretreatment and 1-h post-infection, $\Delta\Delta C_t = 2.84 \pm 0.16$, $n = 3$) or during both the infection and the 4 h post-infection periods ($\Delta\Delta C_t = 5.58 \pm 0.15$, $n = 3$).

Bar graph data are shown as the mean \pm SEM. Data were analyzed using a two-tailed Student's *t*-test. ns: not significant. C_t : threshold cycle, GAPDH: glyceraldehyde 3-phosphate dehydrogenase.

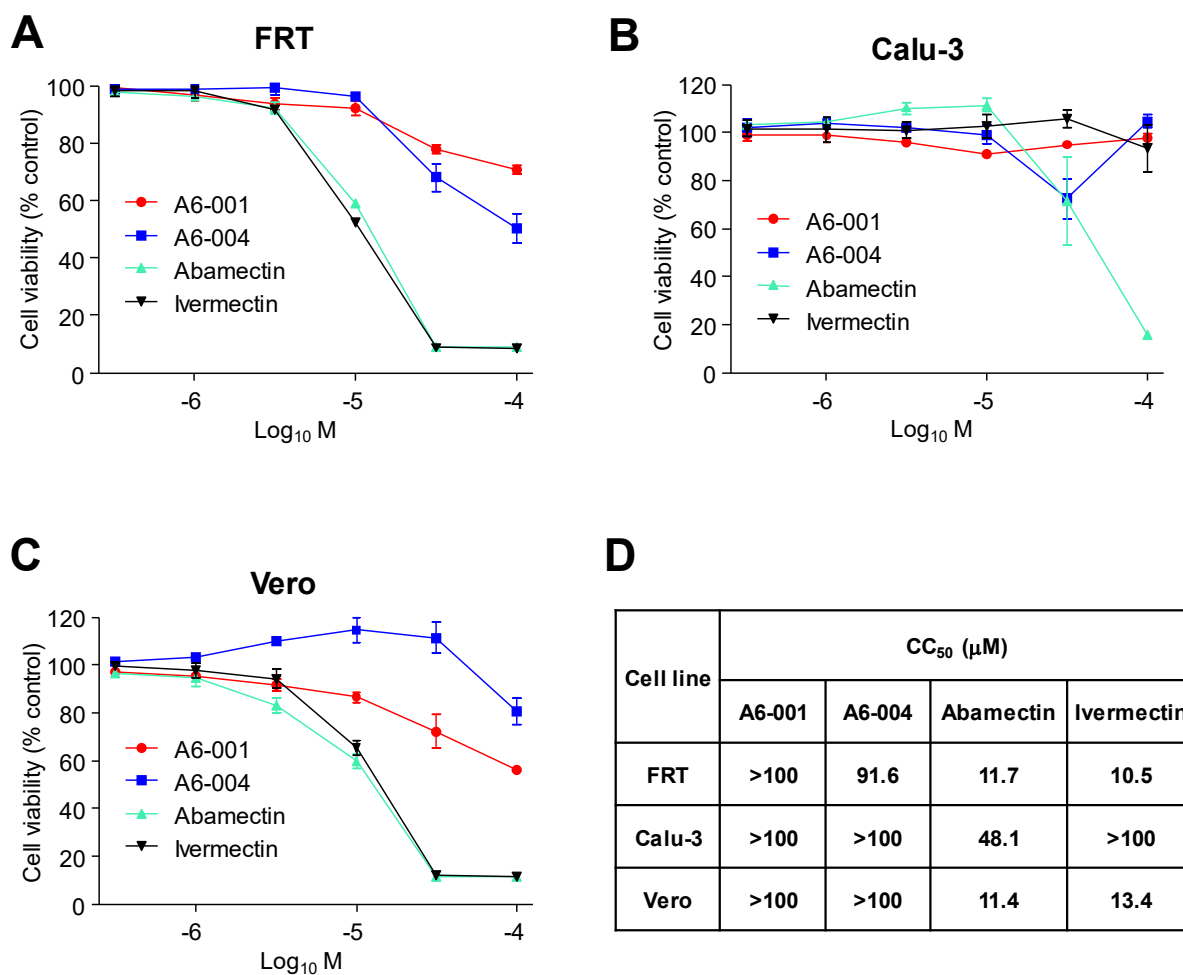


Figure S7. Cell viability analysis of ANO6 inhibitors, Related to Figure 7.

(A-C) FRT (A), Calu-3 (B), and Vero cells (C) were treated with the indicated concentrations of A6-001, A6-004, abamectin, and ivermectin for 48 h. Cisplatin (50 μM) was used as a positive control. Cell viability was determined using the MTS assay (mean ± SEM, n = 6).

(D) The CC₅₀ (the half-maximal cytotoxic concentration) values are summarized.

Table S1. IC₅₀ of ANO6 inhibitors on ANO1, ANO2, and ANO6 anion channels, Related to Figure 1.

	A6-001	A6-004	abamectin	ivermectin
ANO1	41.9 ± 4.8 (460.4)	5.24 ± 0.5 (3.2)	58.1 ± 5.9 (232.4)	29.1 ± 2.7 (29.4)
ANO2	8.20 ± 0.91 (90.1)	0.99 ± 0.10 (0.6)	9.05 ± 0.59 (36.2)	16.9 ± 2.2 (17.1)
ANO6	0.091 ± 0.011	1.64 ± 0.20	0.25 ± 0.06	0.99 ± 0.36

The IC₅₀ values are presented in μM. The numbers in parenthesis represent ANO6 selectivity against each ANO paralog.

Supplemental Videos

Video S1. Time-lapse imaging of HEK 293T-ACE2-TMPRSS2 (Red)/CHO-Control (Green) co-cultures, Related to Figures 4G and 4H

Video S2. Time-lapse imaging of HEK 293T-ACE2-TMPRSS2 (Red)/CHO-Spike (Green) co-cultures, Related to Figures 4G and 4H

Video S3. Time-lapse imaging of HEK 293T-ACE2-TMPRSS2 (Red)/CHO-Spike (Green) co-cultures, A6-001 (10 μ M) treated, Related to Figures 4G and 4H

Video S4. $[Ca^{2+}]_i$ measurement in HEK 293T-ACE2-TMPRSS2 cells: mock vehicle, Related to Figures 5A and 5B

Video S5. $[Ca^{2+}]_i$ measurement in HEK 293T-ACE2-TMPRSS2 cells: SARS2-PsV alone, Related to Figures 5C and 5D

Video S6. $[Ca^{2+}]_i$ measurement in HEK 293T-ACE2-TMPRSS2 cells: BAPTA pretreatment (BAPTA-AM, 3 μ M, 20 min) plus SARS2-PsV, Related to Figures 5E and 5F

Video S7. $[Ca^{2+}]_i$ measurement in HEK 293T-ACE2-TMPRSS2 cells: camostat pretreatment (10 μ M) plus SARS2-PsV, Related to Figures 5G and 5H

Video S8. $[Ca^{2+}]_i$ measurement in HEK 293T-ACE2-TMPRSS2 cells: A6-001 pretreatment (10 μ M) plus SARS2-PsV, Related to Figures 5I and 5J